Cucurbit[7]uril-based Self-assembled Supramolecular Complex with Reversible Multistimuli-Responsive Chromic Behavior and Controllable Fluorescence

Xiao-Feng Wang, Rui-Lian Lin, Wen-Qi Sun, Jing-Xin Liu, Li-Xin Xu*, Carl Redshaw and Xing Feng**

X.-F. Wang, R.-L. Lin, Dr. W.-Q. Sun, Prof. L.-X. Xu, Prof. J.-X. Liu
College of Chemistry and Chemical Engineering, Anhui University of Technology, 1530 Maxiang Road, Maanshan 243002, P. R. China.

Prof. C. Redshaw
Chemistry, School of Natural Sciences, University of Hull, Hull, HU6 7AB, U.K.

Prof. X. Feng
Guangdong Provincial Key Laboratory of Information Photonics Technology, School of Mate rial and Energy, Guangdong University of Technology, Guangzhou 510006, P. R. China.
*E-mail: jxliu411@ahut.edu.cn; lxxu@ahut.edu.cn and hyxhn@sina.com

Keywords: controllable fluorescence, host−guest complex, multistimuli-response, photochromism, thermochromism, vapochromism.

Multistimuli-responsive color-changing materials have potential applications in areas such as chemical sensing and anti-counterfeiting. In this work, a fluoro-phenyl-acetyl-substituted viologen derivative (FPAV·Cl_2) was synthesized, which can form a supramolecular inclusion complex with cucurbit[7]uril (Q[7]) via self-assembly. Significantly, the resulting inclusion complex $FPAV^{2+}$@Q[7] in the solid-state exhibits visual color changes in response to

multiple external stimuli including light, heat, and vapors of ammonia and organic amines. The ESR and UV−vis spectra analysis reveals that the photochromic, thermochromic and vapochromic behavior of $FPAV^{2+}$@Q[7] are due to the generation of $FPAV^{+\bullet}$ free radicals resulting from electron transfer. Furthermore, in the solid-state, $FPAV^{2+}$@Q[7] shows controllable fluorescence regulated by its chromic process. Based on the multistimuli-responsive color-changes and fluorescence properties of $FPAV^{2+}$@Q[7], its practical applications in erasable inkless printing, multiple anti-counterfeiting processes, visible ammonia/organic amines detection, and information encryption were demonstrated. The supramolecular strategy of encapsulating viologen derivatives into macrocycles provides a general method for fabricating multistimuli-responsive chromic materials with multiple practical applications.

1. Introduction

Many living creatures, such as chameleons[1], neon tetra fishes[2], and tree frogs[3], are capable of rapidly changing their color in response to environmental stimuli, including light, temperature, pressure, and moisture. Inspired by the coloration behavior of these organisms, there has been significant effort focused on constructing stimuli-responsive chromic materials.[4-11] Due to their unique physical and chemical signal information, such color-changing materials have promising applications in a broad range of fields from sensors, displays, catalysis, smart windows to anti-counterfeiting processes.[12-21] Among the various stimuli-responsive chromic materials, viologen-based chromic materials are particularly attractive because of their unique electron-deficient properties and excellent chromic performance. Accordingly, a number of viologen-based chromic materials, especially constructed in the form of coordination complexes and polymers, have thus far been developed.[22-36] More often than not, however, most of the reported viologen-based chromic materials only exhibit one or two kinds of stimuli-responsive color changes. The design and

development of a viologen-based multistimuli-responsive chromic material that can undergo multiple color changes upon exposure to various external stimuli is still a considerable challenge given that it usually involves the combination of different functional groups.[37-41]

Our research efforts in this field have focused on the use of supramolecular chemistry. We and others have recently found that by incorporating specific viologen derivatives into macrocyclic hosts, such as cucurbit[*n*]urils or cyclodextrins, viologen-based photochromic materials may be produced.[42-51] Host such as cucurbit[*n*]urils[52-56] and cyclodextrins have inherently rich electronic groups, which may provide electrons to viologen guests, thereby enabling them to achieve chromic performance. On the other hand, after being encapsulated by a macrocyclic host, the viologen guest often exhibits enhanced fluorescence.[57-60] Herein, to develop a reversible multistimuli-responsive chromic material, we have designed a specific viologen guest 1,1'-bis[2-(4-fluorophenyl)-2-oxoethyl]-4,4'-bipyridinium dichloride (fluoro-phenyl-acetyl substituted viologen, abbreviated as FPAV·Cl_2, Figure 1a) and successfully incorporated it into the hydrophobic cavity of cucurbit[7]uril (Q[7], Figure 1b). It should be noted that the acetyl group in the viologen guest is sensitive to Lewis bases, while the electron-withdrawing fluoro group can enhance viologen sensitivity to electron donors.[61] The formed inclusion complexes $FPAV^{2+}$@Q[7] and $FPAV^{2+}$@$Q[7]_2$ in the solid-state exhibited obvious color changes in response to external stimuli namely, light, heat, and vapors of ammonia and organic amines. Here we only discuss $FPAV^{2+}$@Q[7] as an example. For each chromic process, ultraviolet−visible (UV−vis) diffuse reflectance and electron spin resonance (ESR) spectra were recorded and are discussed. Such studies provide insight into the chromic mechanism of the inclusion complex $FPAV^{2+}$@Q[7]. In addition, compared with the viologen guest, the solid-state $FPAV^{2+}$@Q[7] exhibits enhanced fluorescence which can be modulated by the light irradiation time, heating temperature and ammonia/organic amines fumigation time. The application of $FPAV^{2+}$@Q[7] in erasable inkless printing, anti-counterfeiting,

ammomia/organic amines detection, and information encryption were successfully demonstrated.

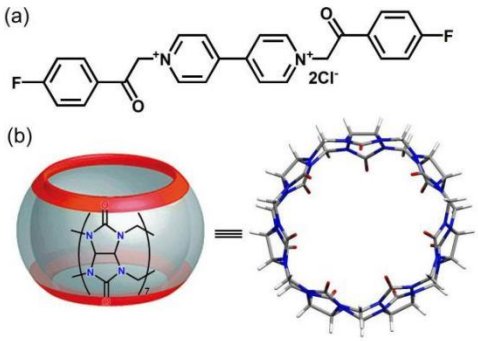

Figure 1. Molecular structures of (a) the viologen guest FPAV·Cl_2 and (b) the host Q[7] used in this work.

2. Results and Discussion

2.1. Host−guest complexation in aqueous solution

Since Q[7] has a large hydrophobic cavity that can accommodate specific organic molecules to form host−guest inclusion complexes, we first investigated the host−guest complexation of Q[7] with $FPAV^{2+}$ in aqueous solution using ^1H NMR spectroscopic titrations. As shown in Figure 2, upon addition of Q[7], the phenyl and oxoethyl proton (H_{cde}) signals of $FPAV^{2+}$ gradually shift upfield, while the pyridinium proton (H_{ab}) signals shift downfield. This observation indicated that the phenyl and oxoethyl units of $FPAV^{2+}$ were encapsulated in the hydrophobic cavity of the Q[7], while its bipyridinium unit was located outside of the portal of the Q[7]. It is possible to form 1:1 binary or 1:2 ternary inclusion complexes of the type $FPAV^{2+}$@Q[7] and $FPAV^{2+}$@$Q[7]_2$ (Scheme 1), respectively, the formation of which depend on the molar ratio of the FPAV·Cl_2 to Q[7] in aqueous solution. Furthermore, in the presence of different concentrations of Q[7], we observed only a single set of proton signals for $FPAV^{2+}$, indicating that the host−guest complexation system quickly exchanges on the ^1H NMR time scale.

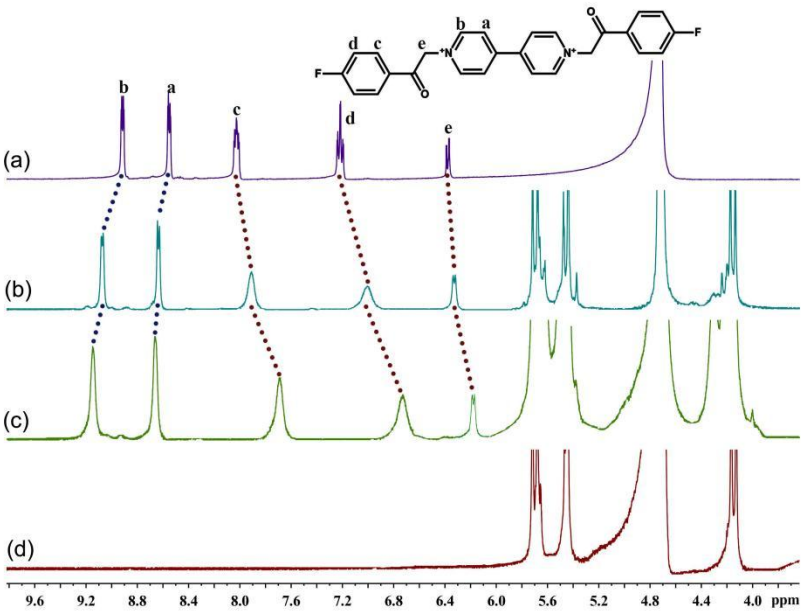

Figure 2. ^{1}H NMR spectra (400 MHz, D_2O) of $FPAV^{2+}$ (2.0 mmol·L^{-1}) in the (a) absence and presence of (b) 0.90 and (c) 2.12 equiv. of Q[7] in D_2O at 20 ºC. (d) shows the ^{1}H NMR spectra (400 MHz, D_2O) of Q[7] in D_2O (2.0 mmol·L^{-1}) at 20 ºC.

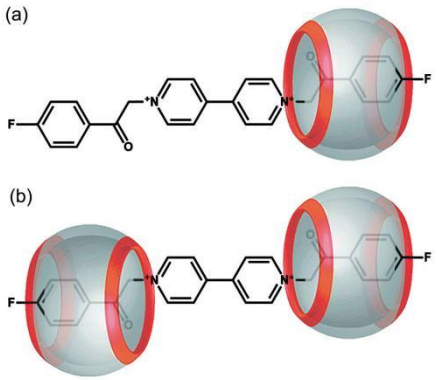

Scheme 1. Schematic view of inclusion complexes (a) $FPAV^{2+}$@Q[7] and (b) $FPAV^{2+}$@$Q[7]_2$.

2D DOSY spectrum of the inclusion complex $FPAV^{2+}$@Q[7] (Figures S4) showed that the host Q[7] and the guest $FPAV^{2+}$ have the same diffusion coefficient ($D = 1.35\times10^{-10}$ m^2·s^{-1}), suggesting they are part of the same species. The diffusion coefficient D of the inclusion complex $FPAV^{2+}$@Q[7] is smaller than that of the free guest ($D = 2.82\times10^{-10}$ m^2·s^{-1}), further

confirming the encapsulation of $FPAV^{2+}$ within Q[7]. To further study the host − guest complexation of Q[7] with $FPAV^{2+}$, isothermal titration calorimetry (ITC) experiments were carried out. The resulting data points (Figure S5) indicate that $FPAV^{2+}$ has double binding to Q[7] and both binding sequences are driven by enthalpy and entropy. According to the data obtained in Figure S4, the binding constants of K_1 and K_2 were calculated to be 9.292×10^8 M^{-1} and 3.323×10^5 M^{-1}, respectively. Using the Klotz equation, one would expect that $K_1 = 4K_2$, assuming equal microscopic binding constants for both sites.[62] However, we observed that $K_1 >> 4K_2$, suggesting considerable negative cooperativity. Clearly, the second binding event is thermodynamically much less favorable than the first one. The formation of the inclusion complexes $FPAV^{2+}$@Q[7] and $FPAV^{2+}$@$Q[7]_2$ was further confirmed by electrospray ionization high resolution mass spectrometry (ESI-MS). Two ions at *m/z* = 796.24067 and *m/z* = 1377.91078 were observed (Figure S6), corresponding to the 1:1 and 1:2 inclusion complexes, respectively. Although the molar ratio of the Q[7] to the $FPAV \cdot Cl_2$ prepared for ESI-MS detection was greater than 2, the observed relative abundance of the 1:1 inclusion complex $FPAV^{2+}$@Q[7] in the ESI-MS was much greater than that of the 1:2 inclusion complex $FPAV^{2+}$@$Q[7]_2$. It may be because that the Q[7] is likely to be separated from the inclusion complexes in the strongly ionized environment of the mass spectrometry tests, which may lead to an increase in signal abundance of 1:1 inclusion complex.

2.2. Photochromic Properties of the Viologen Guest $FPAV \cdot Cl_2$ and Its Inclusion Complex $FPAV^{2+}$@Q[7] in the Solid-State.

No any photochromic behavior was observed for the viologen guest $FPAV \cdot Cl_2$ and its inclusion complex $FPAV^{2+}$@Q[7] in aqueous solution. As can be seen in Figure 3a, upon light irradiation with a 300 W xenon lamp (200 nm-1000 nm) for about 3 minutes, the solid-state viologen guest $FPAV \cdot Cl_2$ changed color from grayish white to pale green. However, the difference in color before and after the color changes was not obvious enough. By contrast,

when the guest FPAV·Cl_2 was encapsulated in the Q[7], the formed inclusion complex $FPAV^{2+}$@Q[7] in the solid-state exhibited an excellent photochromic performance, *i.e.*, the color difference before and after the color changes was far superior, as illustrated in Figure 3b. Before light irradiation, the $FPAV^{2+}$@Q[7] displays a light yellow color. After irradiation with a 300 W xenon lamp for only 5 seconds, the $FPAV^{2+}$@Q[7] showed a naked-eye color change, gradually turning blue, and finally becoming a saturated blue−black within 2 minutes. When the photoproduct of the $FPAV^{2+}$@Q[7] was placed in the dark under air at room temperature, it slowly returned to its original color within 24 hours. These results reveal that the coloration and decoloration process of the $FPAV^{2+}$@Q[7] is reversible.

The photochromic behavior of the $FPAV^{2+}$@Q[7] was monitored by solid-state UV–vis diffuse reflectance and ESR spectroscopy. After irradiation with a 300 W xenon lamp for 2 minutes, the UV–vis absorption spectrum of the $FPAV^{2+}$@Q[7] showed two strong absorption bands centred at 402 and 605 nm (Figure 3c), which likely originate from generated $FPAV^{+\bullet}$ free radicals. We observed that the UV–vis spectrum of the $FPAV^{2+}$@Q[7] also showed a absorption band at 800-1000 nm, which may be attributed to the generation of the radical cationic dimer.[63] The radical dimer deepen the color of solid to dark blue. When the photoproduct of the $FPAV^{2+}$@Q[7] was placed in the dark under air for 24 hours, its UV–vis spectrum almost returned to its original state, indicating that the free radicals were quenched by atmospheric oxygen. Similar to viologen derivatives previously reported in the literature,[37-50] the $FPAV^{2+}$@Q[7] is ESR silent before light irradiation, but exhibits a strong singlet peak (g = 2.0030) after light irradiation (Figure 3d). The ESR signal is attributed to the generation of $FPAV^{+\bullet}$ free radicals, which is presumed to be caused by photo-induced electron transfer from the carbonyl oxygens of the host Q[7] to the pyridinium units of the viologen guest.

For comparison, the UV–vis absorption and ESR spectra of the viologen guest FPAV·Cl_2 in the solid-state were also detected (Figure S7). Obviously, the photochromism of the

FPAV·Cl_2 is also due to the generation of the $FPAV^{+\bullet}$ free radicals, which may be caused by photo-induced electron transfer from the counter anions to the pyridinium units. The FT-IR spectroscopic profile of the $FPAV^{2+}$@Q[7] after light irradiation was essentially identical to that before light irradiation (Figure S8), indicating that the photochromism of the $FPAV^{2+}$@Q[7] was not caused by photocatalysis or structural changes.

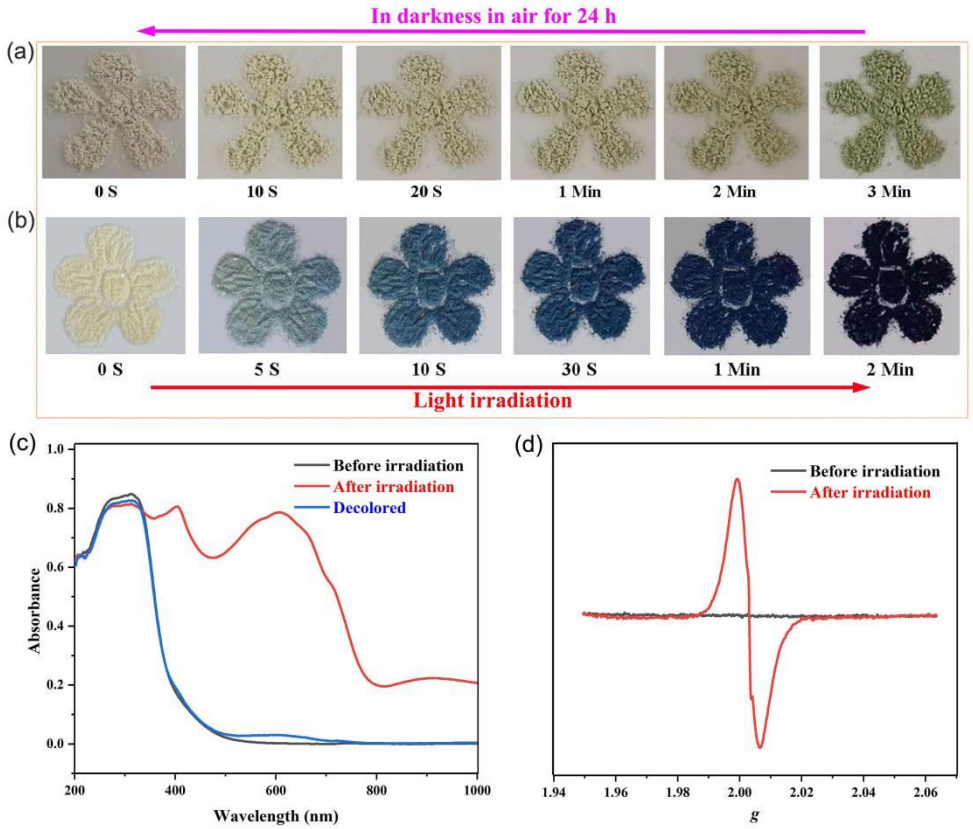

Figure 3. Photographs showing the photochromic behavior of (a) the viologen guest FPAV·Cl_2 and (b) the inclusion complex $FPAV^{2+}$@Q[7] after being irradiated by a 300 W xenon lamp for 3 and 2 minutes, respectively; (c) UV−vis absorption spectra of the solid-state $FPAV^{2+}$@Q[7] before and after light irradiation showing the photochromic behavior; (d) ESR spectra of the solid-state $FPAV^{2+}$@Q[7] before and after light irradiated for about 2 minutes.

2.3. Thermochromic Property of the $FPAV^{2+}$@Q[7] in the Solid State

Strikingly, the solid-state sample of the $FPAV^{2+}$@Q[7] can change color when heated under air. When the $FPAV^{2+}$@Q[7] was heated to 90 °C or higher in the oven without light

irradiation, its color gradually changes from pale yellow to orange−yellow, and then reddish brown (Figure 4a), which depends on the duration and temperature of heating. After being placed in a dark environment under air at room temperature for 12 hours, the reddish brown color of the $FPAV^{2+}$@Q[7] was restored to its original color. When the thermochromic sample was placed in a closed desiccator, it was difficult to observe the decoloration process. However, the thermochromic sample immediately returned to its original pale yellow color when it was fumigated with water vapor. These observations imply that the $FPAV^{2+}$@Q[7] possesses reversible a thermochromic property, and that this reversible thermochromic process is accompanied by dehydration and hydration of the sample. Thermogravimetric analysis (TGA) experiment of the $FPAV^{2+}$@Q[7] (Figure S9) confirms that the weight loss of water is approximately 6.5% of the total weight in the range of 30-140 ^{o}C. To investigate the thermochromic mechanism, UV–vis diffuse reflectance spectra and ESR spectra of the solid-state $FPAV^{2+}$@Q[7] were also recorded before and after heating. As shown in Figure 4b, after heating, the UV–vis diffuse spectrum of the $FPAV^{2+}$@Q[7] exhibited two absorption bands at 410 and 540 nm, corresponding to the reddish brown coloration. Compared with Figure 3b, there is no absorption at 800-1000 nm in Figure 4b, indicating that free radicals initiated by heating cannot form radical cationic dimer. The ESR spectrum of the $FPAV^{2+}$@Q[7] after heating shows a strong resonance with a *g* value of 2.0025 (Figure 4c), indicating that the thermochromism is due to the generation of $FPAV^{+\bullet}$ free radicals via thermo-induced electron transfer.

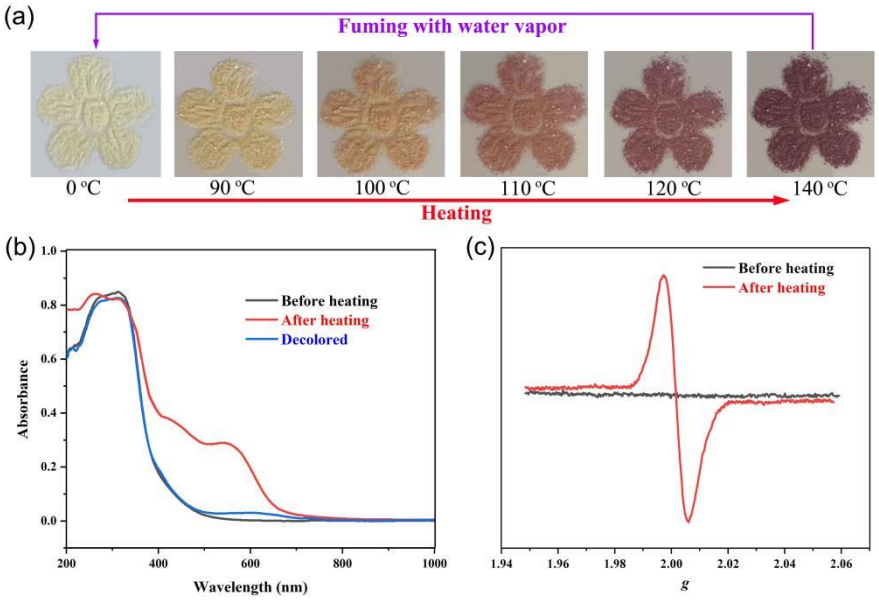

Figure 4. (a) Photographs showing the thermochromic behavior of the $FPAV^{2+}$@Q[7] in different temperature environments; (b) UV−vis absorption spectra of the solid-state $FPAV^{2+}$@Q[7] before and after heat treatment at 140 °C for about 0.5 h showing the thermochromic behavior; (c) ESR spectra of the solid-state $FPAV^{2+}$@Q[7] before and after heat treatment at 140 °C for about 0.5 h.

2.4. Ammonia/Organic Amine Vaporchromism

In addition to responding to light and heat stimuli, the solid-state sample of the $FPAV^{2+}$@Q[7] is also sensitive to volatile ammonia and many organic amines, such as trimethylamine, ethylenediamine, and aniline, and changes color accordingly. As can be seen in Figure 5, upon fuming with ammonia vapor or any of the above mentioned organic amines, the $FPAV^{2+}$@Q[7] exhibited color changes from pale yellow to reddish black or reddish brown, purplish red, and orange−red. The sample color deepened on increasing the ammonia/organic amine fumigation time. The colored samples can fade to the original pale yellow when fumigated with HCl vapor or when standing under air at room temperature for a sufficiently long time. In the absence of Q[7], the solid-state sample of the $FPAV{\cdot}Cl_2$ also exhibited color changes upon fuming with ammonia vapor and organic

amine compounds, but the color change is noticeably weaker than that of the inclusion complex $FPAV^{2+}$@Q[7] (Figure S10). This observation indicate that Q[7] may encapsulate active center and exhibit size selectivity for amine compounds.

After being fumigated with different vapors of ammonia/organic amines, the UV–vis spectra of the $FPAV^{2+}$@Q[7] displayed new absorption bands centred at about 550 nm for ammonia, trimethylamine, and ethylenediamine, and at about 410 nm for aniline (Figure 6a). The ESR spectra of the colored samples exhibited single signals with g values of approximately 2.003 (Figure 6b). The new absorption bands in the UV–vis spectra and single signals in the ESR spectra indicate the generation of $FPAV^{+\bullet}$ free radicals. As is well known, there are lone pair electrons on the nitrogen atom of ammonia or organic amines. Given that the pyridinium unit of the $FPAV^{2+}$ is electron-deficient, it can accept electrons from electron-rich ammonia/organic amines, thereby forming donor-acceptor interactions between the $FPAV^{2+}$ and the ammonia/organic amines. Therefore, we observed that the $FPAV^{2+}$@Q[7] responds to the stimulus of ammonia/organic amines and changes its own color. In addition, the ammonia vapor atmosphere produced the fastest and deepest coloration, while the aniline vapor atmosphere produced the slowest and least noticeable coloration. The difference in the color changes is due to different steric hindrance of the substituents associated with ammonia and the organic amines. The small ammonia readily approaches the pyridinium unit, and effectively transfers electrons to the pyridinium unit. By contrast, the somewhat larger aniline, having the greatest steric hindrance (benzene ring), prevents effective contact between the electron-rich and electron-deficient groups. As a result, the electron transfer requires more time to trigger and is less effective.

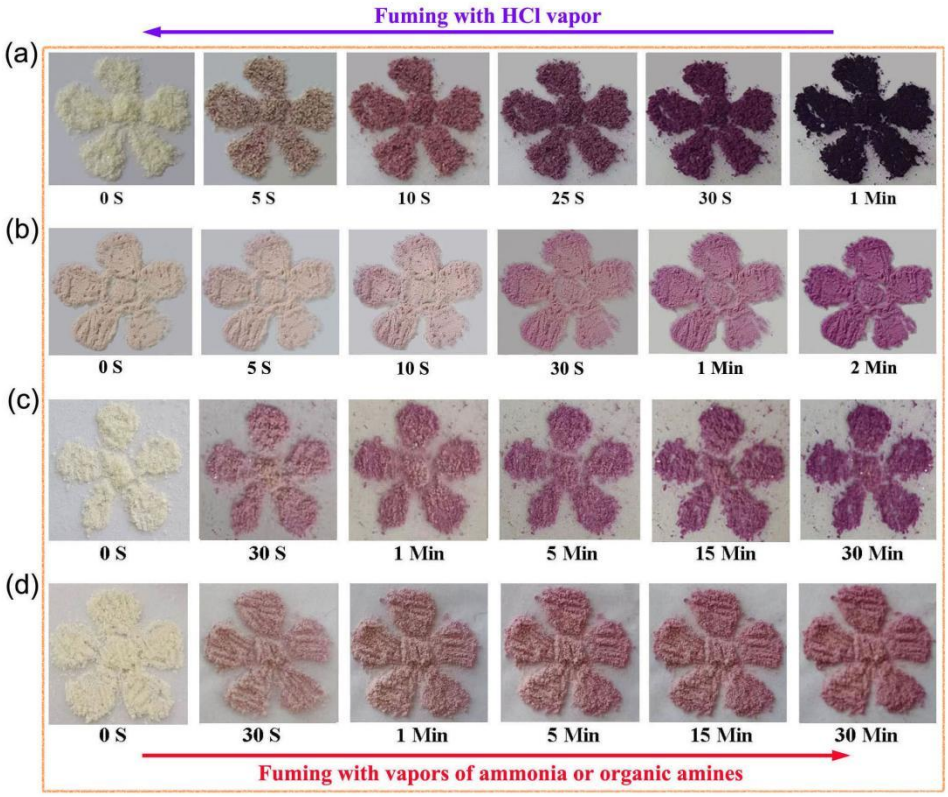

Figure 5. Photographs showing the color changes of the $FPAV^{2+}$@Q[7] upon fuming with vapors of (a) ammonia, (b) trimethylamine, (c) ethylenediamine, (d) aniline for different durations.

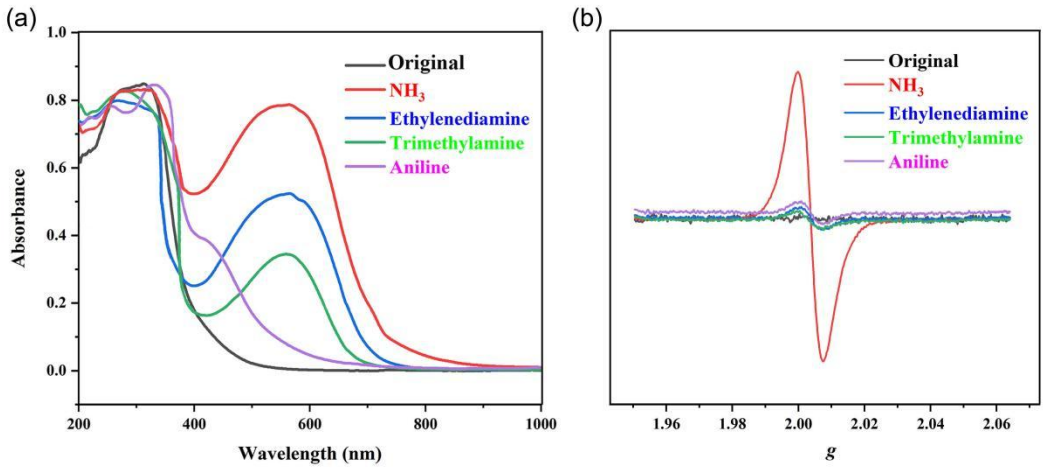

Figure 6. (a) UV−vis absorption and (b) EPR spectra of the solid-state $FPAV^{2+}$@Q[7] fumigated with vapors of ammonia and organic amines for about 0.5 h.

As mentioned above, although the photochromic, thermochromic and vapochromic

behavior of $FPAV^{2+}$@Q[7] is due to the production of $FPAV^{+\bullet}$ free radicals caused by electron transfer; their color changes are distinctly different from each other. This phenomenon can be attributed to two reasons, firstly that the electron donors or electron providing methods used for chromic behavior are significantly different. The photochromic behavior of $FPAV^{2+}$@Q[7] is caused by photo-induced electron transfer, its thermochromic behavior is caused by thermo-induced electron transfer, and its vapochromic behavior is caused by the ammonia/organic amines donating electrons. Secondly, that the components of the color changing products are different. Essentially, the photochromic process of the $FPAV^{2+}$@Q[7] involves only electron transfer, its thermochromic process involves dehydration, while its vapochromic process involves vapor adsorption.

2.5. Controllable Fluorescence Emission

The viologen guest $FPAV{\cdot}Cl_2$ shows photoluminescence when dissolved in aqueous solution. In the solid-state, it affords very weak fluorescence because of the aggregation-causing quenching effect originating from the π−π stacking of the fluorophores in $FPAV{\cdot}Cl_2$. Nevertheless, we observed that the solid-state sample of the $FPAV{\cdot}Cl_2$ exhibited interesting emission enhancement when encapsulated by Q[7]. Furthermore, the fluorescence intensity of the $FPAV^{2+}$@Q[7] is related to the light irradiation time. As shown in Figure 7a, solid-state $FPAV{\cdot}Cl_2$ initially emits baby blue fluorescence under lab UV light (λ_{ex} = 365 nm). After irradiation with a 300 W xenon lamp, the solid-state $FPAV^{2+}$@Q[7] gradually turned blue-black and its fluorescence intensity gradually decreased. After irradiation for 2 minutes, the color change of the $FPAV^{2+}$@Q[7] reached saturation, and its emission was quenched by 80% (Figure 7b). Once the $FPAV^{2+}$@Q[7] is placed in darkness and restored to its original color, its fluorescence emission also returns to its original intensity. The solid-state photoluminescence spectra suggest that the fluorescence intensity depends on the

photochromic process and can be modulated by the light irradiation time. The observed fluorescence quenching can be attributed to the transformation of the emissive molecules into non-emissive radical species upon light irradiation.

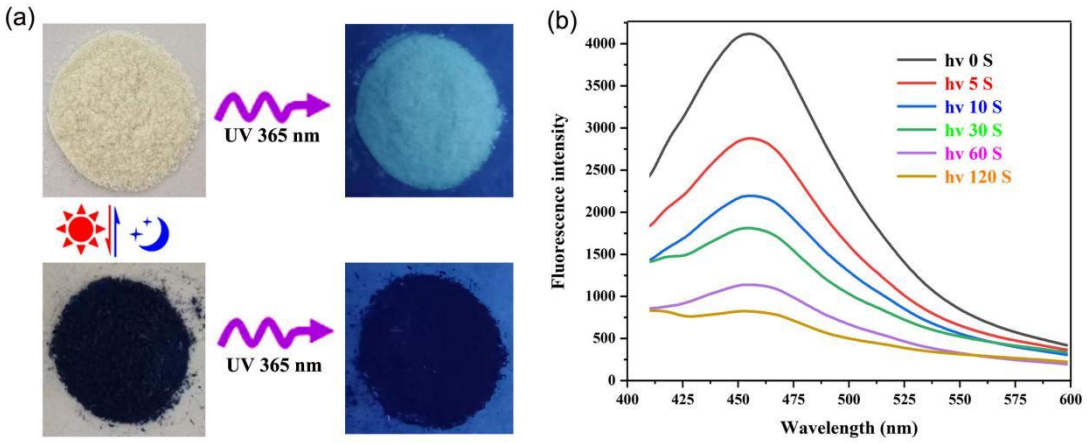

Figure 7. (a) Photographs showing the difference in fluorescence for $FPAV^{2+}$@Q[7] before and after light irradiation; (b) Fluorescence spectrum of $FPAV^{2+}$@Q[7] changed during the light irradiation process.

The solid-state fluorescence emission can also be modulated by the thermochromic and vapochromic processes because the generated free radicals lead to fluorescence quenching or fluorescence weakening. As shown in Figure S11, the fluorescence emission is also sensitive to the stimuli of heat and ammonia/organic amines vapor. Moreover, the fluorescence intensity can also be regulated by the heating temperature and ammonia/organic amine fumigation time.

2.6. Application in Inkless Printing, Anti-Counterfeiting, Ammonia/Organic Amine Detecting and Information Encryption

In comparison with the multistimuli-responsive chromic materials previously reported [37-41], the solid-state $FPAV^{2+}$@Q[7] demonstrates distinct advantages. Firstly, the solid-state $FPAV^{2+}$@Q[7] is easily prepared through self-assembly. Secondly, the solid-state

$FPAV^{2+}$@Q[7] shows high response speed because its chromic behavior is essentially caused by electron transfer. The performances of the solid-state $FPAV^{2+}$@Q[7] prompted us to explore its potential applications. Using a previously reported method,[28, 39, 43-45, 64, 65] we prepared cellulose filter paper coated with $FPAV^{2+}$@Q[7]. As shown in Figure 8a, the target patterns can be repeatedly "printed" on the filter paper by using a customized mask and light irradiation for 2 minutes with a 300 W xenon lamp. The "printed" pattern persists for at least 6 h at room temperature. Under UV light (λ_{ex} = 365 nm), the "printed" pattern is clearly visible. A two-dimensional code (QR code) with digital information can also be "printed" on the filter paper (Figure 8b). Under both daylight and 365 nm UV light, the "printed" QR code is recognizable by the naked eye and decodable by a smart phone, endowing such "printed" QR codes with multiple anti-counterfeiting functions. Moreover, the $FPAV^{2+}$@Q[7] coated filter paper can be used for detecting ammonia/organic amine leakage. As shown in Figure 8c, the filter paper showed significant color changes in response to the vapors of different ammonia/organic amines, which is consistent with the behavior of the solid-state sample of $FPAV^{2+}$@Q[7]. In particular, in an ammonia vapor atmosphere, the filter paper showed a rapid visible color change in less than 10 seconds.

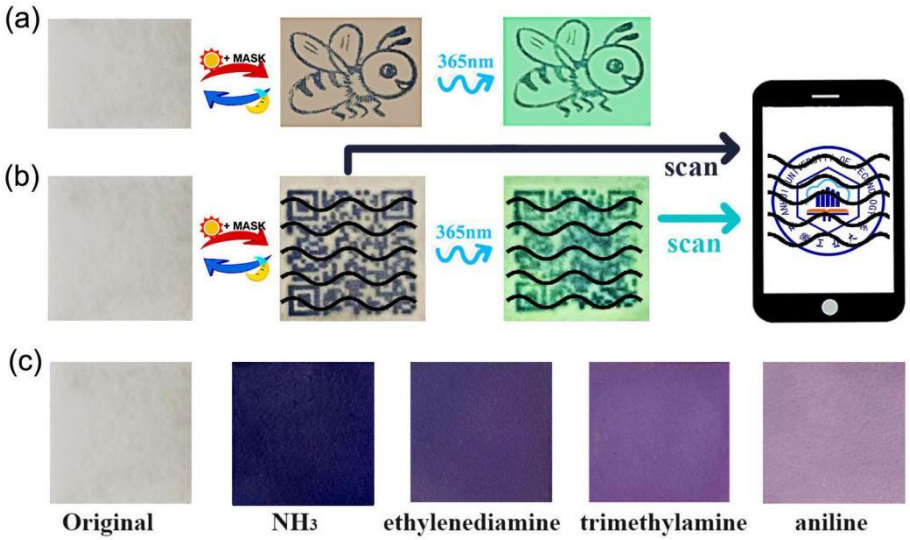

Figure 8. (a) Photograph showing that the pattern of a bee is "printed" on the filter paper coated with $FPAV^{2+}$@Q[7]; (b) A QR code "printed" on the filter paper can be recognized by

a smart cell phone under daylight and a lab UV light; (c) Photographs showing the color changes of the filter paper coated with the $FPAV^{2+}$@Q[7] after exposure to different amine vapors.

We also designed an information encryption and decryption system by using the fluorescence and photochromic properties of $FPAV^{2+}$@Q[7]. As interpreted in Figure 9a, two types of filter papers coated with $FPAV^{2+}$@Q[7] and $FPAV{\cdot}Cl_2$ are placed in a dot-matrix (4 × 8) grid. The emissive or photochromic output is defined as "1", and if there is no output, it is defined as "0". Under daylight, all the dots are assigned a value of "0", and we obtain an invalid code. Under UV light (λ_{ex} = 365 nm), 11 dots of the $FPAV^{2+}$@Q[7]-coated filter paper emitted light blue fluorescence (Figure 9b). The first-level information is directly deciphered as "AHUT" (Anhui University of Technology) by transforming the binary code to American Standard Code for Information Interchange (ASCII) code. Under the light irradiation of a 300 W xenon lamp, 12 dots of the filter papers changed their color to blue-black (8 dots) or green (4 dots). The second-level information can be deciphered as "CHEM". To obtain the encrypted information, one needs not only the correct decoding book, but also the right operation method and sequence.

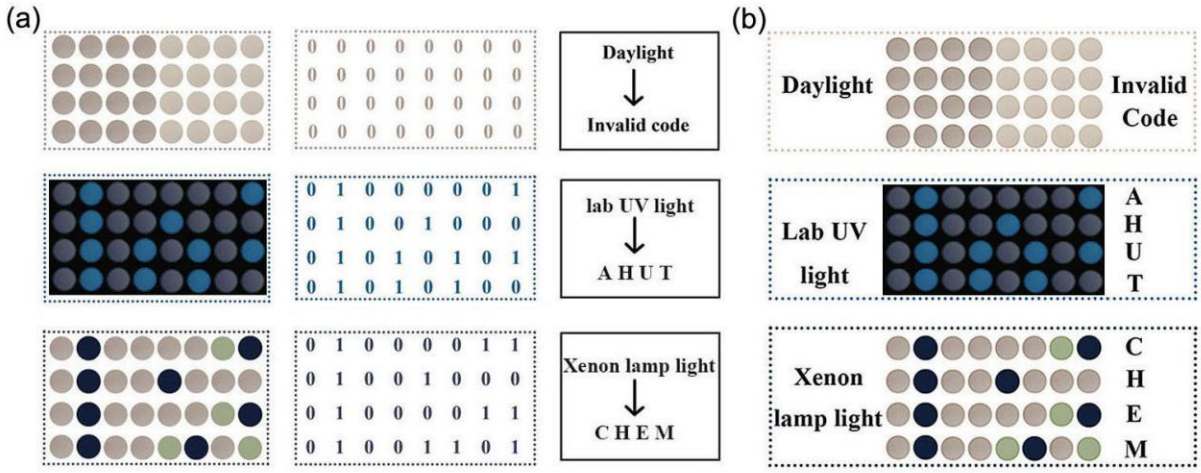

Figure 9. (a) Schematic illustration of the information encryption and decryption process based on different light sources; (b) Photographs showing that the dot-matrix patterns provide decrypted information on "AHUT" and "CHEM" under a lab UV light (λ_{ex} = 365 nm) and a 300 W xenon lamp light.

3. Conclusion

In conclusion, a 1:1 molar ratio inclusion complex of the macrocycle Q[7] bound with the fluoro-phenyl-acetyl-substituted viologen FPAV·Cl_2 was constructed by self-assembly. The inclusion complex $FPAV^{2+}$@Q[7] in the solid-state shows naked-eye color changes in response to multiple stimuli, including light, heat, and vapors of ammonia and organic amines. The ESR and UV−vis diffuse reflectance spectra of the $FPAV^{2+}$@Q[7] for different chromic processes all suggest that the color changes or chromism originate from the generation of $FPAV^{+\bullet}$ free radicals caused by electron transfer. In addition, solid-state $FPAV^{2+}$@Q[7] exhibited strong fluorescence emission, the intensity of which can be modulated by the chromic process. Based on the multistimuli-responsive properties, a triple-function paper was prepared to demonstrate the practical application of the inclusion complex $FPAV^{2+}$@Q[7] in erasable inkless printing, multiple anti-counterfeiting and visible ammonia/organic amine detection. The combination of the photochromic behavior and fluorescence property of the $FPAV^{2+}$@Q[7] make it applicable to information encryption. This work provides a new strategy for constructing multistimuli-responsive chromic materials for the promising applications in one area after another.

4. Experimental Methods

4.1. Materials and characterization: The macrocyclic host Q[7] was synthesized according to the methods of Kim and co-workers.[56] The starting materials for synthesizing the viologen guest FPAV·Cl_2 were purchased from Aladdin and used directly without further purification.

NMR spectral measurements were carried out on a Bruker DPX 400 spectrometer. High resolution mass spectrometry (HRMS) was performed on an Agilent 6540 Q-TOF mass spectrometer (Agilent Technologies, Inc., Santa Clara, CA). Ultraviolet–visible (UV–vis) diffuse reflectance spectra were recorded on a Shi-madzu UV3600 UV–vis spectrophotometer equipped with an integrating sphere in the wavelength range of 200−1000 nm. Electron-spin resonance (ESR) spectra were measured by using a Bruker A300 spectrometer. FT-IR spectra were recorded on a Nicolet Magna 750 spectrometer using KBr disks in the range of 4000−450 cm^{-1}. A CEL-HXF300 xenon lamp system was used for photochromic tests. The distance between the sample and the Xe lamp was set at 50 cm. Fluorescence spectra in both solid-state and aqueous solutions were recorded on a Varian Cary Eclipse spectrofluorometer (Varian, Inc., Palo Alto, CA, USA). The thermal gravimetric analyses (TGA) were carried out on a SHIMADZU DTG-60 instrument under N_2 atmosphere with a heating rate of 10 $^oC\ min^{-1}$.

4.2. Isothermal titration calorimetry (ITC) experiments: ITC experiments were performed on a Nano ITC instrument (TA, USA). All solutions were prepared in purified water and degassed prior to titration experiments. A typical ITC titration was carried out by titrating Q[7] solution into a FPAV·Cl_2 solution. The heat evolved was recorded at T = 298.15 K. Curve fitting were performed using the Nano ITC analyze software. The independent model were used to analyzed the data. The enthalpy and entropy values obtained in the ITC experiments were used to calculate the change in Gibbs free energy ΔG and the binding constant (K) by the standard relationship

$$\Delta G = -RT \ln K = \Delta H - T\Delta S$$

where R is the gas constant.

4.3. Synthesis of FPAV·Cl_2: 1,1'-Bis[2-(4-fluorophenyl)-2-oxoethyl]-4,4'-bipyridinium dichloride (FPAV·Cl_2): 4,4'-bipyridine (0.20 g, 1.28 mmol) and 2-chloro-4'-

fluoroacetophenone (0.51 g, 2.95 mmol) were dissolved in DMF (20 mL). The mixed solution was heated to 45 °C and refluxed for about 24 h. The produced precipitate was filtered and washed with acetone 5 times to afford FPAV·Cl_2 (0.37 g, 68%). M.p.: 218.6 °C. FT-IR (KBr, cm^{-1}): 3383, 3052, 3006, 2926, 2839, 1636, 1596, 1558, 1505, 1349, 1240, and 852. ^{1}H NMR (400 MHz, DMSO-d6) δ 9.40 (d, *J* = 6.4 Hz, 1H), 8.99 (d, *J* = 6.4 Hz, 1H), 8.36 – 8.14 (m, 1H), 7.58 (t, *J* = 8.7 Hz, 1H), 6.70 (s, 1H). ^{13}C NMR (101 MHz, DMSO-d6) δ 190.08 (s), 168.12 (s), 165.57 (s), 150.90 (s), 147.09 (s), 131.52 (d, *J* = 10.1 Hz), 129.36 (s), 126.87 (s), 116.59 (s), 116.37 (s), 66.70 (s). HRMS (ESI, in H_2O) *m/z* calcd for $FPAV^{2+}$ ($C_{26}H_{20}N_2O_2F_2^{2+}$-$H^+$) 429.141 (100.0%)/430.145 (28.9%)/431.148 (4.0%), found 429.139. The characterization spectra of FPAV·Cl_2 are shown in Figures S1 and S2.

4.4. Preparation of solid-state samples of the inclusion complex $FPAV^{2+}$@Q[7]: The macrocyclic host Q[7] (0.053 g, 0.046 mmol) and the viologen guest FPAV·Cl_2 (0.02 g, 0.046 mmol) were dissolved in 10 mL water. The mixed aqueous solution was stirred and heated at 60 °C for about 10 min. After removing the water through vacuum-rotary evaporation, we obtained the solid product $FPAV^{2+}$@Q[7]. Yield 100%. The solubility of the obtained $FPAV^{2+}$@Q[7] is 7.14 grams in 100 g water. The melting point of the inclusion complex $FPAV^{2+}$@Q[7] (M.p.: 363-365 °C) is much larger than that of the FPAV·Cl_2 (M.p.: 218.6 °C). ^{1}H NMR (400 MHz, D_2O) δ 9.16 (s, 1H), 8.67 (s, 1H), 7.70 (s, 1H), 6.74 (s, 1H), 6.27 (s, 1H), 5.67 (dd, *J* = 22.9, 15.1 Hz, 10H), 5.46 (d, *J* = 13.4 Hz, 10H), 4.53 – 3.95 (m, 10H). FT-IR (KBr, cm^{-1}): 3443, 3072, 3005, 2939, 2390, 1743, 1472, 1421, 1375, 1328, 1232, 1190, 1030, 965, 803, 758, 675, 626 and 570. Compared with that of the viologen guest FPAV·Cl_2, the FT-IR spectrum of the inclusion complex $FPAV^{2+}$@Q[7] displays specific vibration absorptions of the Q[7], including the stretching vibration absorption of C═O at 1743 cm^{-1} and the bending vibration absorption of C─H at 965 cm^{-1}. The characterization spectra of the inclusion complex $FPAV^{2+}$@Q[7] are shown in Figures S3.

4.5. DOSY NMR Experiments: The DOSY NMR experiments were performed on a Bruker

DPX 400 spectrometer at 25 °C with a pulsed-gradient stimulated echo sequence, using bipolar gradients.[66] The 2D DOSY spectra were generated by using the program GIFA software.[67] The diffusion coefficient *D* is given by the Stokes−Einstein equation[68, 69]:

$$D = \frac{kT}{6\pi\eta R_{\mathrm{H}}}$$

where *k* is the Boltzmann constant, η is the solvent viscosity, and R_{H} is the hydrodynamic radius of the detected compound.

Supporting Information

Supporting Information is available from the Wiley Online Library or from the author.

Acknowledgements

The authors are grateful for the support from the National Natural Science Foundation of China (Grant No. U22A20408), the Natural Science Foundation of Anhui Province (1808085MB43), and the Natural Science Research Project of Anhui Province Education Department (2023AH040150). CR thanks the University of Hull for support.

Received: ((will be filled in by the editorial staff))
Revised: ((will be filled in by the editorial staff))
Published online: ((will be filled in by the editorial staff))

References

1. J. Teyssier, S. V. Saenko, D. Van Der Marel, M. C. Milinkovitch, *Nat. Commun.* **2015**, *6*, 6368.
2. D. Gur, B. A. Palmer, B. Leshem, D. Oron, P. Fratzl, S. Weiner, L. Addadi, *Angew. Chem. Int. Ed.* **2015**, *54*, 12426.
3. H. N. Skold, S. Aspengren, M. Wallin, *Pigm. Cell Melanoma Res.* **2013**, *26*, 29.

4. Y. Matsuo, Y. Wang, H. Ueno, T. Nakagawa, H. Okada, *Angew. Chem. Int. Ed.* **2019**, *58*, 8762.
5. Q.-K. Wang, G. Ligorio, V. Diez-Cabanes, D. Cornil, B. Kobin, J. Hildebrandt, M. C. Nardi, M. Timpel, S. Hecht, J. Cornil, E. L. List-Kratochvil, N. Koch, *Adv. Funct. Mater.* **2018**, *28*, 1800716.
6. M. Lahav, M. E. van der Boom, *Adv. Mater.* **2018**, *30*, 1706641.
7. H. Zhang, X. Wu, *Adv. Sci.* **2016**, *3*, 1500224.
8. Y.-S. Mi, H.-B. Cheng, H.-Q. Chu, J. Zhao, M.-M. Yu, Z.-J. Gu, Y.-L. Zhao, L.-L. Li, *Chem. Sci.* **2019**, *10*, 10231.
9. Y.-J. Ma, J.-X. Hu, S.-D. Han, J. Pan, J.-H. Li, G.-M. Wang, *J. Am. Chem. Soc.* **2020**, *142*, 2682.
10. N.-N. Zhang, R.-J. Sa, S.-S. Sun, M.-D. Li, M.-S. Wang, G.-C. Guo, *J. Mater. Chem. C.* **2019**, *7*, 3100.
11. C. Sun, X.-Q. Yu, M.-S. Wang, G.-C. Guo, *Angew. Chem. Int. Ed.* **2019**, *58*, 9475.
12. C. Li, A. Iscen, H. Sai, K. Sato, N. A. Sather, S. M. Chin, Z. Alvarez, L. C. Palmer, G. C. Schatz, S. I. Stupp, *Nat. Mater.* **2020**, *19*, 900.
13. L. Jia, B. B. Zhang, J. Xu, T. H. Zhu, R. J. Chen, F. Zhou, *ACS Appl. Mater. Interfaces* **2020**, *12*, 19955.
14. Y. H. Yang, J. Z. He, Z. He, G. H. Jiang, *Adv. Opt. Mater.* **2021**, *9*, 2001584.
15. T. Gong, Q. Sui, P. Li, X.-F. Meng, L.-J. Zhou, J.-Q. Chen, J.-H. Xu, L. Wang, E.-Q. Gao, *Small* **2019**, *15*, 1803468.
16. M. M. Paquette, B. O. Patrick, N. L. Frank, *J. Am. Chem. Soc.* **2011**, *133*, 10081.
17. C. Chen, J.-K. Sun, Y.-J. Zhang, X.-D. Yang, J. Zhang, *Angew. Chem., Int. Ed.* **2017**, *56*, 14458.
18. Z. Li, N. Song, Y.-W. Yang, *Matter.* **2019**, *1*, 345.
19. J.-R. Wu, G. Wu, D. Li, Y.-W. Yang, *Angew. Chem. Int. Ed.* **2023**, e202218142.

20. M. Zhang, W. Zhao, *Aggregate* **2021**, *2*, e60.

21. Q. Wang, Z. Qi, M. Chen, D.-H. Qu, *Aggregate* **2021**, *2*, e110.

22. G. P. Li, L. T. Xu, W. D. Zhang, K. Zhou, Y. S. Ding, F. L. Liu, X. M. He, G. He, *Angew. Chem.Int. Ed.* **2018**, *57*, 4897.

23. C. Chen, J.-K. Sun, Y.-J. Zhang, X.-D. Yang, J. Zhang, *Angew. Chem.Int. Ed.* **2017**, *56*, 14458.

24. X. J. Sun, J. Zhang, Z. Y. Fu, *ACS Appl. Mater. Interfaces.* **2018**, *10*, 35671.

25. H. J. Chen, G. M. Zheng, M. Li, Y. F. Wang, Y. Song, C. H. Han, J. C. Dai, Z. Y. Fu, *Chem. Commun.* **2014**, *50*, 13544.

26. T. Gong, P. Li, Q. Sui, J. Chen, J. Xu, E.-Q. Gao, *J. Mater. Chem. A.* **2018**, *6*, 9236.

27. Y. C. Shi, J. Liu, M. Li, J. M. Zheng, C. Y. Xu, *Electrochim. Acta.* **2018**, *285*, 415.

28. C.-M. Yu, P.-H. Wang, Q. Liu, L.-Z. Cai, G.-C. Guo, *Cryst. Growth Des.* **2021**, *21*, 1323.

29. M. Chang, D. Liang, F. Zhou, H. Xue, H. Zong, W. Chen, G. Zhou, *ACS Appl. Mater. Interfaces* **2022**, *14*, 15448.

30. Y.-J. Zhang, C. Chen, B. Tan, L.-X. Cai, X.-D. Yang, J. Zhang, *Chem. Commun.* **2016**, *52*, 2835.

31. S.-L. Li, M. Li, Y. Zhang, H.-M. Xu, X.-M. Zhang, *Inorg. Chem.* **2020**, *59*, 9047.

32. R.-G. Lin, G. Xu, G. Lu, M.-S. Wang, P.-X. Li, G.-C. Guo, *Inorg. Chem.* **2014**, *53*, 5538.

33. P.-X. Li, M.-S. Wang, L.-Z. Cai, G.-E. Wang, G.-C. Guo, *J. Mater. Chem. C.* **2015**, *3*, 253.

34. C.-C. Ko, V. W.-W. Yam, *Acc. Chem. Res.* **2018**, *51*, 149.

35. A. M. Rice, C. R. Martin, V. A. Galitskiy, A. A. Berseneva, G. A. Leith, N. B. Shustova, *Chem. Rev.* **2020**, *120*, 8790.

36. X. Li, J.Yang, Y.-W. Yang, *Mater. Chem. Front.* **2023**, *7*, 1463.

37. S.-L. Li, M. Han, Y. Zhang, G.-P. Li, M. Li, G. He, X.-M. Zhang, *J. Am. Chem. Soc.* **2019**, *141*, 12663.

38. X.-N. Li, Z.-M. Tu, L. Li, Z.-H. Wang, H. Zhang, *Dalton Trans.* **2020**, *49*, 3228.

39. D.-D. Yang, H.-W. Zheng, Y.-H. Fang, Q.-F. Liang, Q.-Z. Han, Y.-S. Shi, X.-J. Zheng, *Inorg. Chem.* **2022**, *61*, 7513.

40. T. Zhou, J. Chen, T. Wang, H. Yan, Y. Xu, Y. Li, W. Sun, *ACS Appl. Mater. Interfaces.* **2022**, *14*, 57037.

41. M. Hu, F. Xing, Y. Zhao, Y.-L. Bai, M.-X. Li, S. Zhu, *ACS Omega.* **2017**, *2*, 1128.

42. Q. Wang, M. C. Liu, W. Q. Sun, R. L. Lin, J. X. Liu, *New J. Chem.* **2021**, *45*, 22249.

43. Q. Wang, M. C. Liu, W. Q. Sun, R. L. Lin, R. G. Lin, J. X. Liu, *J. Phys. Chem. C.* **2022**, *126*, 844.

44. Q. Wang, J. Z. Guo, C. Zhang, W. Q.Sun, R. L. Lin, M. F. Ye, *J. X. Liu, J. Phys. Chem. C* **2022**, *126*, 18900.

45. D.-X. Xia, L.-W. Fan, M. F. Ye, W.-Q. Sun, R. L. Lin, J.-X. Liu, *Mater. Adv.* **2023**, *4*, 5215.

46. Q. Wang, J. Z. Guo, D. Luo, M. F. Ye, R. L. Lin, W. Q. Sun, J. X. Liu, *Phys. Chem. Chem. Phys.* **2022**, *24*, 25930.

47. Q. Wang, X.-F. Wang, W.-Q. Sun, R.-L. Lin, M.-F. Ye, J.-X. Liu, *ACS Appl. Mater. Interfaces.* **2023**, *15*, 2479.

48. L.-J. Wu, R. Fu, G. Huang, R.-L. Lin, J.-X. Liu, *ACS Appl. Opt. Mater.* **2023**, *1*, 1811.

49. D. Sun, Y. Wu, X. Han, S. Liu, *Mater. Chem. Front.* **2022**, *6*, 2929.

50. H. Nie, Y. Rao, J. Song, X.-L. Ni, *Chem. Mater.* **2022**, *34*, 8925.

51. D. Kim, A. Aktalay, N. Jensen, K. Uno, M. L. Bossi, V. N. Belov, *S. W. Hell, J. Am. Chem. Soc.* **2022**, *144*, 14235.

52. J. Lagona, P. Mukhopadhyay, S. Chakrabarti, L. Isaacs, *Angew. Chem., Int. Ed.* **2005**, *44*, 4844.

53. K. I. Assaf, W. M. Nau, *Chem. Soc. Rev.* **2015**, *44*, 394.

54. Y. Huang, R. H. Gao, X. L. Ni, X. Xiao, H. Cong, Q. J. Zhu, K. Chen, Z. Tao, *Angew.*

Chem., Int. Ed. **2021**, *60*, 15166.

55. J. X. Liu, K. Chen, C. Redshaw, *Chem. Soc. Rev.* **2023**, *52*, 1428.
56. J. Kim, I. S. Jung, S. Y. Kim, E. Lee, J. K. Kang, S. Sakamoto, K. Yamaguchi, K. Kim, *J. Am. Chem. Soc.* **2000**, *122*, 540.
57. Y. Xia, S. Chen, X.-L. Ni, *ACS Appl. Mater. Interfaces.* **2018**, *10*, 13048.
58. T. Jiang, X. Wang, J. Wang, G. Hu, X. Ma, *ACS Appl. Mater. Interfaces.* **2019**, *11*, 14399.
59. Q. Wang, K. Zhang, R. L. Lin, W.-Q. Sun, M. F. Ye, X. Xiao, J.-X. Liu, *Org. Biomol. Chem.* **2022**, *20*, 1253.
60. H. Nie, Z. Wei, X.-L. Ni, Y. Liu, *Chem. Rev.* **2022**, *122*, 9032.
61. W. Shi, F. Xing, Y.-L. Bai, M. Hu, Y. Zhao, M.-X. Li, S. Zhu, *ACS Appl. Mater. Interfaces* **2015**, *7*, 14493.
62. I. M. Klotz, D. L. Hunston, *Biochemistry* **1971**, *10*, 3065.
63. B. Tang, W.-L. Li, Y. Chang, B. Yuan, Y. Wu, M.-T. Zhang, J.-F. Xu, J. Li, X. Zhang, *Angew. Chem. Int. Ed.* **2019**, *58*, 15526.
64. B. Garai, A. Mallick, R. Banerjee, *Chem. Sci.* **2016**, *7*, 2195.
65. Q. Shi, S.-Y. Wu, X.-T. Qiu, Y.-Q. Sun, S.-T. Zheng, *Dalton Trans.* **2019**, *48*, 954.
66. A. Jerschow, N. Muller, *J. Magn. Reson.* **1997**, *125*, 372.
67. J. L. Pons, T. E. Malliavin, M. A. Delsuc, *J. Biomol. NMR* **1996**, *8*, 445.
68. S. Floquet, S. Brun, J.-F. Lemonnier, M. Henry, M.-A. Delsuc, Y. Prigent, E. Cadot, F. Taulelle, *J. Am. Chem. Soc.* **2009**, *131*, 17254.
69. B. Chen, J. J. Holstein, S. Horiuchi, W. G. Hiller, G. H. Clever, *J. Am. Chem. Soc.* **2019**, *141*, 8907.